# U.S. Summer Precipitation and Temperature Patterns Following the Peak Phase of El Niño

HUI WANG

*Climate Prediction Center, NOAA/NWS/NCEP, College Park, Maryland, and Wyle Science, Technology and Engineering Group, McLean, Virginia*

ARUN KUMAR AND WANQIU WANG

*Climate Prediction Center, NOAA/NWS/NCEP, College Park, Maryland*

BHASKAR JHA

*Climate Prediction Center, NOAA/NWS/NCEP, College Park, Maryland, and Wyle Science, Technology and Engineering Group, McLean, Virginia*

(Manuscript received 11 November 2011, in final form 18 May 2012)

ABSTRACT

Evidence for spatially coherent, but different, U.S. summer precipitation and surface air temperature anomalies during the evolving phase and during the summers following the peak phase of the winter El Niño is presented. The spatial patterns during the decaying phase of El Niño are distinctive from patterns in the preceding summer when El Niño is in its evolving phase, that is, the traditional ''simultaneous'' composite patterns associated with El Niño. The analysis of a multimodel ensemble of global atmospheric models forced by observed sea surface temperature further confirms that the differences in the U.S. summer precipitation and surface temperature anomalies between the developing and decaying phases of El Niño are a result of the atmospheric response to tropical warm SST anomalies that are shifted eastward and are confined east of 120°W during the decaying phase of El Niño. Given the distinctive pattern, and relatively large amplitude of these anomalies during the decaying phase of El Niño, the results may have implications for the seasonal prediction of U.S. summer precipitation and temperature following winter El Niños.

## 1. Introduction

El Niño–Southern Oscillation (ENSO) affects U.S. precipitation not only in winter but also in summer (e.g., Ropelewski and Halpert 1986, 1987). The relationship between U.S. summer precipitation and tropical Pacific sea surface temperature (SST) has received considerable attention for decades. For example, an empirical study of Bunkers et al. (1996) indicated that summer precipitation in the northern plains is closely related to the variability of ENSO SST. Trenberth and Guillemot (1996) linked the Great Flood of 1993 in the Midwest to SST forcing in the tropical Pacific. They argued that the tropical heating associated with El Niño in 1993 altered the large-scale circulation over the Pacific and North American region and helped build the persistence of heavy precipitation in the Midwest. A recent study by Weaver et al. (2009) demonstrated that El Niño–related SST anomalies can increase warm season precipitation over the central United States through enhancement in the Great Plains low-level jet.

Although our understanding of the ENSO influence on U.S. summer precipitation has been greatly improved in the past few decades, some puzzling discrepancies with respect to the ENSO-related U.S. precipitation pattern also remain. Figure 1a shows June–August (JJA) seasonal mean U.S. precipitation anomalies from a composite of 12 El Niño years, which are defined based on the Niño-3.4 SST anomaly (Barnston et al. 1997; Trenberth 1997) and selected from the 1950–2005 period (see section 2). In this composite, summer precipitation associated with

*Corresponding author address:* Dr. Hui Wang, NOAA/Climate Prediction Center, 5830 University Research Court, College Park, MD 20740.
E-mail: hui.wang@noaa.gov

DOI: 10.1175/JCLI-D-11-00660.1

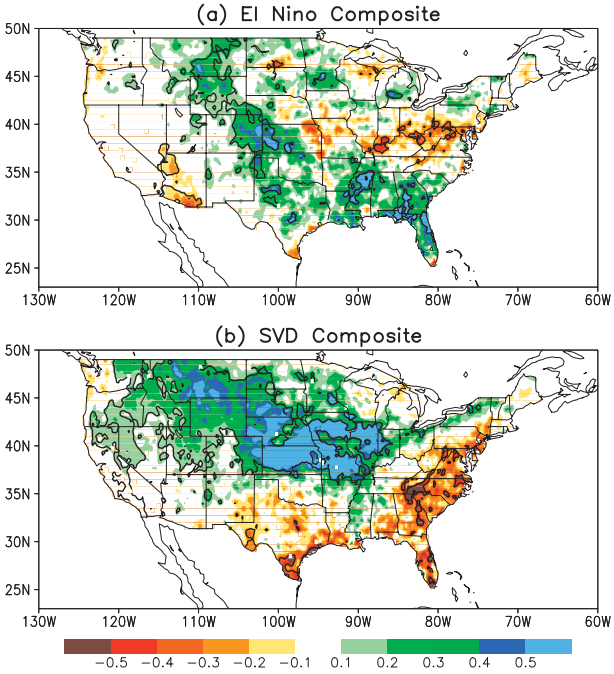


FIG. 1. Composites of June–August (JJA) seasonal mean precipitation anomaly (mm day$^{-1}$) based on observational data for (a) 12 El Niño summers and (b) 12 summers in the first SVD mode that covary with El Niño (Wang et al. 2010). The anomalies circled by thick black lines are above the 95% significance level estimated by the Monte Carlo test.

El Niño is above normal in the Southeast and Great Plains, and below normal in the Ohio River basin. A similar composite pattern of U.S summer precipitation can also be found at the NOAA Climate Prediction Center (NOAA/CPC) website (http://www.cpc.ncep.noaa.gov/products/precip/CWlink/ENSO/composites/EC_ENP_index.shtml).

Following a different approach and using 41-yr (1950–90) observational data and the singular value decomposition (SVD) method (Bretherton et al. 1992), Ting and Wang (1997) identified a U.S. summer precipitation pattern as the first SVD mode that covaries with the tropical ENSO SST, but is different from the El Niño composite of precipitation anomalies in Fig. 1a. The result of Ting and Wang was reproduced with longer records (60 yr, 1948–2007) of observations (Wang et al. 2010). Figure 1b shows such a precipitation pattern, which is a composite of U.S. summer precipitation for the 12 summers selected when projection coefficients for the tropical Pacific SST projected onto the first SVD mode documented in Wang et al. (2010) were greater than 0.7. In these 12 years, U.S. summer precipitation displays strong covariance with the El Niño–like SST (Wang et al. 2010, their Figs. 6a,b). The precipitation pattern in Fig. 1b is characterized by above-normal precipitation in the Midwest and northern plains, and below-normal precipitation in the Atlantic states and along the Gulf Coast. In some regions the precipitation anomalies in Fig. 1b are opposite to those in Fig. 1a, such as in the Southeast and southern plains.

The inconsistency between the El Niño composite of U.S. summer precipitation and the composite of precipitation covarying with El Niño based on the SVD analysis (Ting and Wang 1997; Wang et al. 2010) may arise from different years selected for the two composites. The El Niño composite (Fig. 1a) likely represents a forced precipitation response to the tropical Pacific SST, whereas the SVD composite (Fig. 1b) could pick up on modes of precipitation that are covarying with the tropical Pacific SST and are linked through an atmospheric circulation, but are not necessarily connected via a causal mechanism. To what extent do both composites represent a causal mechanism linking El Niño SST to the U.S. summer precipitation anomalies? The question is important from the perspective of identifying sources of seasonal predictability and may be answered through Atmospheric Model Intercomparison Project (AMIP) simulations in which SST is prescribed as a boundary forcing.

An ENSO cycle has a phase-locking behavior with a peak phase occurring typically in boreal winter (Neelin et al. 2000). Therefore, in summertime if the SST anomalies in the tropical Pacific are on the warmer side, it is likely that they either correspond to a developing phase of El Niño (leading to the peak phase in the following winter) or in a decaying phase following the El Niño winter. Kumar and Hoerling (2003) found an asymmetry in the strength of tropical–extratropical teleconnection between the summers preceding and following the peak phase of ENSO, with a stronger circulation response in the following than in the preceding summer. It was suggested that the asymmetry is due to a delayed circulation response to the ENSO SST anomalies. In the present study, we will show that such an asymmetry also exists in the summertime U.S. precipitation and surface temperature response to El Niño between the developing and decaying phases and accounts for the difference between Figs. 1a and 1b.

The present study aims to explore physical explanations for the inconsistency between Figs. 1a and 1b through observational and modeling analyses. Improved understanding of the forcing mechanisms for the observed precipitation anomalies could provide guidance for summer seasonal precipitation prediction. This paper is organized as follows: section 2 provides a description of the datasets and the AMIP simulations used. Sections 3 and 4 examine causal connection between the U.S. summer precipitation and surface temperature patterns and SST anomalies in the observations and AMIP simulations, respectively. Conclusions are given in section 5.

TABLE 1. List of 12 El Niño years and the 12 years covarying with El Niño in the first SVD mode (Wang et al. 2010) used for compositing U.S. summer precipitation in Figs. 1a,b, respectively. Both 12-yr sets are broken down into seven overlapping years and five nonoverlapping years. Four summers (bold) out of the five nonoverlapping years in the SVD composite followed four El Niño events (italic) in the seven overlapping years. Values in parentheses are the normalized projection coefficients for summer (JJA) tropical Pacific SST projected onto the first SVD mode.

| Composite type | Both composites: seven overlapping years | El Niño composite: five nonoverlapping years | SVD composite: five nonoverlapping years |
|---|---|---|---|
| Year | *1957* (1.48) | 1963 (0.32) | 1951 (0.78) |
| | 1965 (1.02) | 1991 (0.65) | **1958** (0.84) |
| | 1972 (1.31) | 1994 (0.28) | **1983** (2.25) |
| | *1982* (0.92) | 2002 (0.51) | **1993** (1.23) |
| | 1987 (1.61) | 2004 (0.47) | **1998** (0.93) |
| | *1992* (1.03) | | |
| | *1997* (3.24) | | |

## 2. Data

The data used in this study consist of precipitation, surface air temperature, 200-hPa geopotential height, and SST from both observations and atmospheric general circulation model (AGCM) simulations forced by the observed SSTs. For observations, the U.S. precipitation data are taken from the NOAA/CPC Unified Precipitation for 1950–98 and from the real-time U.S. daily precipitation analysis for 1999–2005 (Higgins et al. 2000), both on a $0.25° \times 0.25°$ (latitude $\times$ longitude) grid. The U.S. surface air temperatures are from the NOAA merged land–ocean surface temperature dataset (Smith et al. 2008) on a $5° \times 5°$ grid. The 200-hPa heights are from the National Centers for Environmental Prediction–National Center for Atmospheric Research (NCEP–NCAR) reanalysis (Kalnay et al. 1996). The SSTs are from the NOAA extended reconstructed SST version 3b dataset (ERSST v3b) (Smith et al. 2008) on a $2° \times 2°$ grid.

Observational analysis is limited in its ability to separate the SST-forced precipitation variability from other sources, for example, due to atmospheric internal variability, and, therefore, it is difficult to establish a causal relationship between precipitation and SST based on the observational data alone. This shortcoming can be overcome by analyzing ensemble results of AMIP simulations with appropriate SST prescribed as a boundary forcing. It has been demonstrated that an ensemble of AMIP simulations can effectively increase the signal-to-noise ratio and obtain reliable ENSO-forced atmospheric signals in the extratropics (Kumar and Hoerling 1995).

To infer the atmospheric responses to the tropical Pacific SST, simulations from four AGCMs forced with the observed time-varying global SST from 1950 to 2005 are used in this analysis. The AGCMs are the Max-Planck Institute ECHAM4.5 (Roeckner et al. 1996), the Geophysical Fluid Dynamics Laboratory AGCM version 3 (GFDL-3) (Delworth et al. 2006), the National Aeronautics and Space Administration Seasonal-to-Interannual Prediction Project AGCM (NSIPP-1) (Bacmeister et al. 2000), and the atmospheric component of the NCEP Climate Forecast System version 2 (CFSv2) (Saha et al. 2010). The four models subjected to observed time-varying SSTs were integrated from 1949 to 2005 with 24, 10, 9, and 9 realizations, respectively. Each realization started from a different initial condition with the first year (1949) discarded as the spinup phase. Our analysis focuses on the multimodel ensemble of 52 members over the 1950–2005 period.

Composite analysis is applied to precipitation, surface air temperature, SST, and 200-hPa geopotential height fields. The El Niño years are chosen using the definition in Trenberth (1997) that the 5-month running mean SST anomaly in the Niño-3.4 region (5°S–5°N, 120°–170°W) is greater than 0.4°C and lasts for more than six months, and additionally, among which at least two months are summer months (JJA). The SVD composite are based on the first SVD mode of the U.S. summer precipitation and Pacific SST in Wang et al. (2010, their Figs. 6 and 7). This mode captures the summer U.S. precipitation anomalies covarying with the ENSO SST in the tropical Pacific. The summers with normalized projection coefficients greater than 0.7 for the tropical Pacific SST projected onto this mode are selected for the SVD composite. The statistical significance of the composite anomalies is estimated by the Monte Carlo technique (e.g., Wilks 1995).

## 3. Observational analysis

To determine how different the years are in compositing U.S. summer precipitation anomalies between Figs. 1a and 1b, Table 1 lists both 12 years used for the El Niño composite based on the Niño-3.4 SST and the SVD composite covarying with the tropical Pacific SST depicted by the first SVD mode in Wang et al. (2010). There are seven El Niño years that are common between the two sets of 12 years including 1957, 1965, 1972, 1982, 1987,

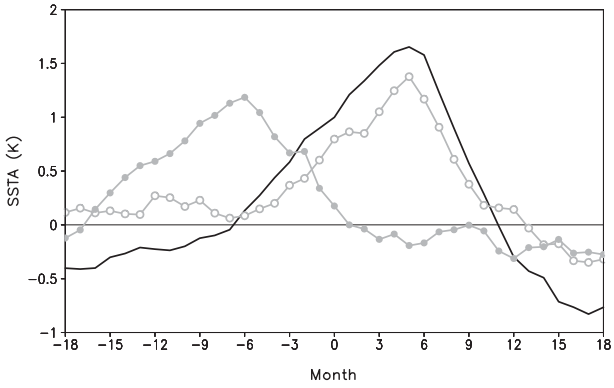


FIG. 2. Composites of Niño-3.4 SST anomalies in observations for the seven overlapping (black) and five nonoverlapping (gray with open circles) summers used in the El Niño precipitation composite (Fig. 1a), as well as the five nonoverlapping summers (gray with solid dots) used in the SVD precipitation composite (Fig. 1b). They correspond to the developing phase of the eastern Pacific (EP) El Niño, central Pacific (CP) El Niño, and the decaying phase (DP) of the eastern Pacific El Niño, respectively, defined later in section 3. The composite time series are from January of previous year (month −18) to January of the following year (month 18). Month 0 corresponds to July of current year.

1992, and 1997. The five nonoverlapping years for the El Niño composite are 1963, 1991, 1994, 2002, and 2004. Four of them are in the most recent two decades. It is also noted that for the SVD composite, four out of five nonoverlapping years lag the above overlapping El Niño years, and are actually during the decaying phase of El Niño. They are 1958, 1983, 1993, and 1998. The projection coefficient for summer tropical Pacific SST projected onto the first SVD mode is also listed in Table 1 for each year, based on which the years for the SVD composite (Fig. 1b) are selected. Consistently, the five nonoverlapping years for the El Niño composite have small projection coefficients ($<0.7$).

Figure 2 shows the composite time series of monthly mean Niño-3.4 SST anomalies from January of the previous year to January of the following year for both overlapping and nonoverlapping events, with month 0 corresponding to July of the current year. The composite time series of Niño-3.4 SST anomalies for both seven overlapping and five nonoverlapping summers used in the El Niño composite (Fig. 1a) display a maximum SST anomaly in the winter following the July (month 0). It indicates that these summers are in the developing phase of El Niño. For the five nonoverlapping summers in the SVD composite (Fig. 1b), a peak of warm SST anomalies occurs in the previous winter, suggesting that these summers are in the decaying phase of El Niño. Therefore, the El Niño composite (Fig. 1a) consists of 12 summers, all in the developing phase of El Niño, whereas the SVD composite (Fig. 1b) consists of 12 summers out of which 7 are in the developing phase and 5 in the decaying phase. It is noteworthy that the amplitude of the JJA (i.e., months −1, 0, and +1 in Fig. 2) Niño-3.4 SST anomalies during the decaying phase is smaller than that during the developing phase by 0.86°C.

It would be interesting to understand why the first SVD mode in Wang et al. (2010) captures the U.S. summer precipitation variability associated with tropical Pacific SST variations, but some of them are in the developing phase of El Niño while others in the decaying phase, and why some other summers also in the developing phase are excluded from this SVD mode. Figure 3 presents the composites of Pacific SST and U.S. precipitation anomalies for the seven overlapping and five nonoverlapping summers used in the El Niño composite (Fig. 1a), as well as the five nonoverlapping summers in the SVD composite.

The composite SST pattern for the seven overlapping summers (Fig. 3a) displays a typical canonical El Niño SST distribution with the largest warm SST anomalies in the tropical eastern Pacific, weak warm SST anomalies along the west coast of North America, and cold SST anomalies in the western and central North Pacific. In contrast, the composite SST pattern for the five nonoverlapping El Niño summers (Fig. 3b) is characterized by warm SST anomalies in the tropical central Pacific and also warm SST anomalies across the North Pacific basin. The SST pattern in Fig. 3b is similar to the central Pacific El Niño or El Niño Modoki (Ashok et al. 2007), which has been documented to occur more frequently in the 1990s and 2000s (Yeh et al. 2009). The warm SST anomalies of the five nonoverlapping summers used in the SVD composite (Fig. 3c) are confined to the east of 120°W, consistent with the withdrawal of warm SST anomalies during the decaying phase of El Niño. For convenience, the SST anomalies in the eastern Pacific (EP) during the developing phase (Fig. 3a), in the central Pacific (CP, Fig. 3b), and in the eastern Pacific during the decaying phase (DP, Fig. 3c) are hereafter referred to as EP, CP, and DP El Niños, respectively.

Since both EP and CP El Niños (Figs. 3a,b) show relatively large SST anomalies in the Niño-3.4 region (5°S–5°N, 120°–170°W), these 12 summers are picked out for the El Niño precipitation composite (Fig. 1a). On the other hand, both EP and DP El Niños (Figs. 3a,c) show strong SST anomalies in the tropical eastern Pacific, which are highly projected onto the first SVD mode in Wang et al. (2010). These 12 summers are thus picked up in the SVD-based analysis of Wang et al. and used for the SVD composite (Fig. 1b). From this comparison it is clear that the different years selected in compositing U.S. summer precipitation in Figs. 1a,b are due to an inclusion of different years that are associated with the

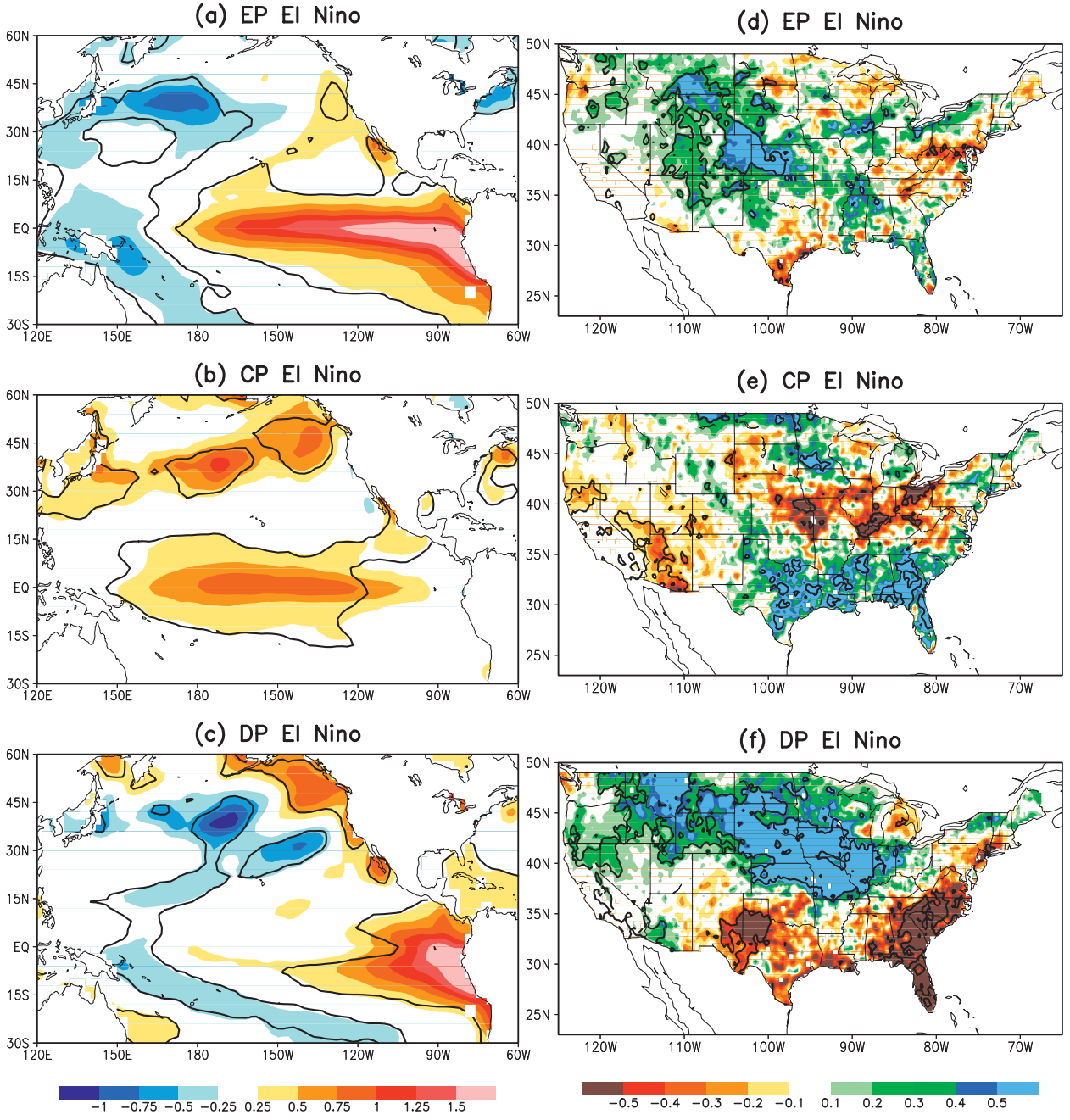


FIG. 3. Composites of (left) JJA seasonal mean Pacific SST (°C) and (right) U.S. precipitation (mm day$^{-1}$) anomalies in observations for (a),(d) the seven overlapping (EP) and (b),(e) five nonoverlapping (CP) El Niños used in the El Niño composite and (c),(f) five nonoverlapping (DP) El Niños used in the SVD composite. The anomalies circled by thick black lines are above the 95% significance level estimated by the Monte Carlo test.

CP El Niño and the DP El Niño in respective precipitation composites.

Associated with the EP El Niño (Fig. 3a), summer precipitation is generally above normal over most of the United States with some dry spots in Texas and the Mid-Atlantic states (Fig. 3d). Associated with the CP El Niño (Fig. 3b), U.S. summer precipitation is dominated by a tripole pattern with positive precipitation anomalies in the Southeast and Texas, negative anomalies in the central United States between 37° and 42°N, and positive anomalies farther to the north (Fig. 3e). Both precipitation patterns in Figs. 3d,e contribute to the El Niño

composite of precipitation anomalies in Fig. 1a. The spatial structure of the precipitation pattern in Fig. 3f is similar to that in Fig. 1b but is stronger in amplitude, suggesting that precipitation anomalies in the decaying phase of El Niño are stronger than those in the developing phase, and thus dominate the SVD composite (Fig. 1b). This is consistent with the stronger circulation response in the summer following an ENSO winter than in the summer preceding the ENSO winter due to a delayed circulation response to ENSO (Kumar and Hoerling 2003).

Changes in summer surface air temperature are closely related to precipitation anomalies (Zhao and Khalil 1993). Composites of summer surface temperature anomalies associated with the three El Niño categories are shown in Fig. 4. During the EP El Niño, surface temperature is generally colder than normal across most of the United States (Fig. 4a). Associated with the CP El Niño, temperature is warmer in the Northeast and West, but statistical significance is less (Fig. 4b). During the DP El Niño, temperature displays a dipole pattern with warm anomalies in the southern states and to the south of Great Lakes and cold anomalies in the northern plains and eastern Pacific Northwest (Fig. 4c). Overall, temperature anomalies in Figs. 4a,c are negatively correlated with precipitation anomalies in Figs. 3d,f, respectively, consistent with the finding of Zhao and Khalil (1993). To summarize, the JJA temperature anomalies for the three El Niño categories have distinct spatial patterns consistent with the corresponding precipitation anomalies.

To assess possible changes in the atmospheric response to the tropical SST, Figs. 5a–c present the composite of 200-hPa height anomalies for different phases/patterns of El Niño. The circulation associated with the EP El Niño (Fig. 5a) is characterized by positive height anomalies in the tropics, with maxima in the central and eastern Pacific, and a wave train from the tropical Pacific to the extratropics in both hemispheres. This is the typical circulation pattern in response to the El Niño SST. Associated with the CP El Niño, the maxima in the tropical Pacific shift westward (Fig. 5b), consistent with the warm SST anomalies in the equatorial central Pacific (Fig. 3b). During the decaying phase of El Niño, in contrast, the maxima shift eastward (Fig. 5c), consistent with the warm SST distribution in Fig. 3d. In addition, the positive height anomalies in the tropics are stronger, with a broader meridional extension, during the decay phase of El Niño than during the developing phase, consistent with the delayed response to ENSO in Kumar and Hoerling (2003).

Figures 5d–f show the same composite of 200-hPa height anomalies in the North Pacific and North American region after removing the zonal mean component. The height anomalies in Fig. 5d exhibit a well-defined

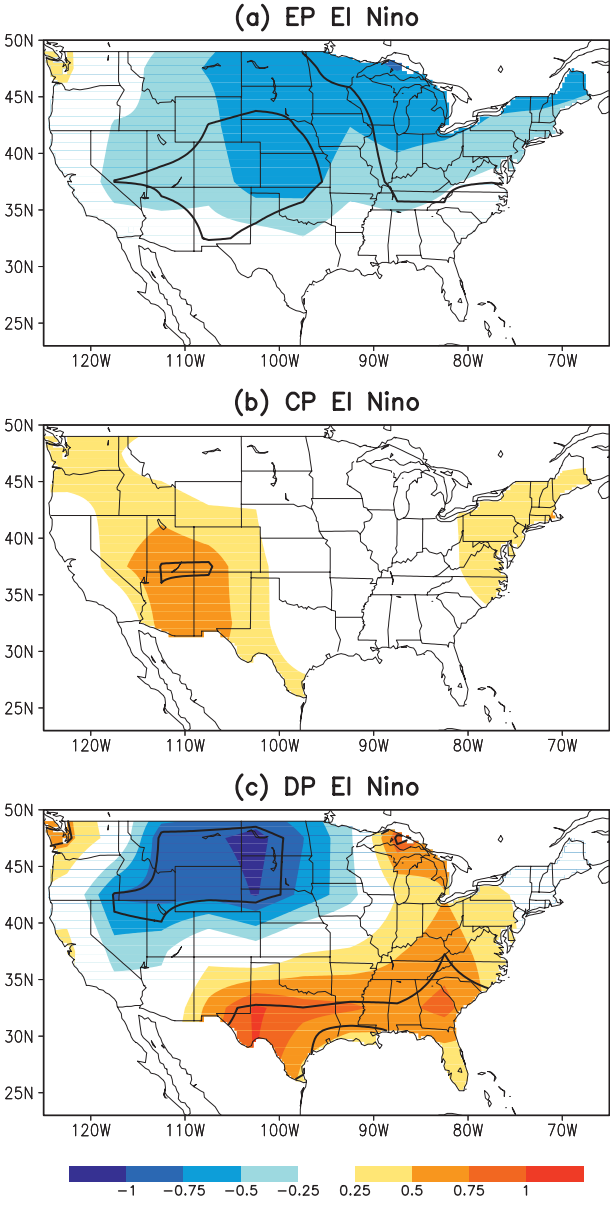


FIG. 4. As in Fig. 3, but for JJA seasonal mean U.S. surface air temperature anomaly (°C) in observations.

teleconnection pattern associated with the tropical heating. The negative height anomalies on the California coast and positive anomalies in the central United States indicate an onshore flow in California and a southeasterly flow from the Gulf of Mexico, consistent with above-normal precipitation in the Northern Rocky Mountain and Great Plains (Fig. 3d). The configuration of the height anomalies in central Canada suggests northerly flow across the U.S.–Canadian border, leading to cold temperature anomalies in the northern United States (Fig. 4a). Similarly, associated with the CP El Niño, it can be inferred that the negative height anomalies in the United States

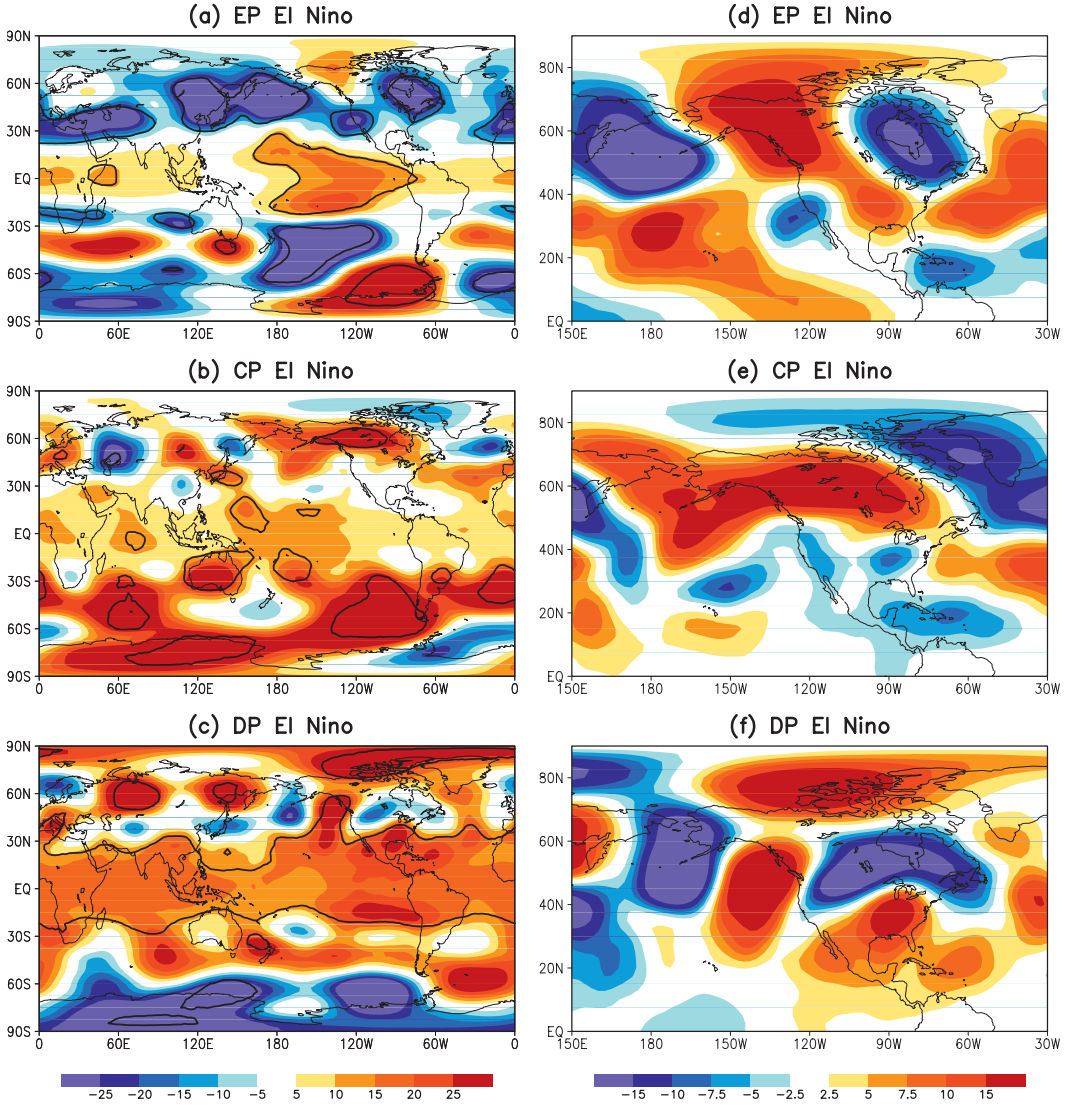


FIG. 5. As in Fig. 3, but for (left) observed JJA seasonal mean global 200-hPa geopotential height anomaly (gpm) and (right) the 200-hPa height anomaly in the North Pacific and North America after removing corresponding zonal means.

(Fig. 5e) are likely responsible for the above-normal precipitation in the Gulf States (Fig. 3e) and warm temperature anomalies in the west (Fig. 4b). The positive height anomalies over the eastern United States and negative anomalies over Canada in Fig. 5f in the decaying phase of El Niño are also consistent with the patterns of precipitation and temperature anomalies in Figs. 3f and 4c. Therefore, the shift of SST anomalies, associated tropical heating, and extratropical circulation response to this shift help interpret the difference in the U.S. summer precipitation and temperature associated with different SST patterns during the developing and decaying phases of El Niño.

## 4. Analysis of AMIP simulations

The observational analysis of the El Niño and SVD-based composites presented so far is based on a small sample size (e.g., precipitation composites in Figs. 3d,e,f, respectively, only rely on seven, five, and five events). Further, for the SVD-based analysis that keys on maximizing the covariability between SST and precipitation, the causality of SST as the forcing for precipitation over the United States is not ensured. AMIP simulations forced by observed SST are, therefore, employed to assess whether precipitation anomalies in Figs. 3d–f are the responses to the different tropical Pacific SST anomalies

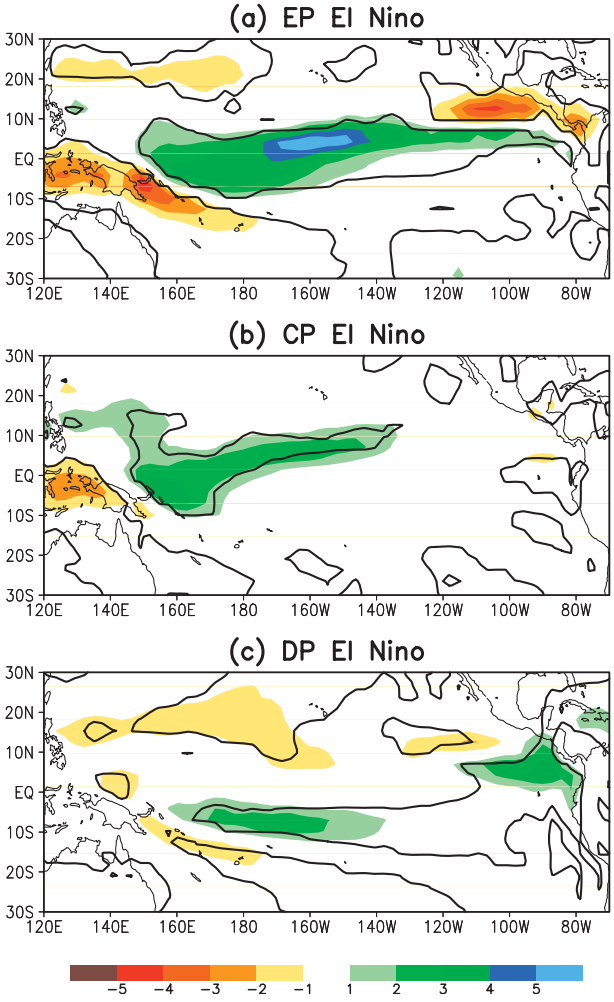


FIG. 6. As in Fig. 3, but for JJA seasonal mean precipitation anomaly (mm day$^{-1}$) in the tropical Pacific from the multimodel ensemble of 52 AMIP simulations.

in Figs. 3a–c, and also to provide more atmospheric realizations than can be gleaned from observational data alone. Although the use of AMIP runs does not increase the sample size of El Niño events, within a limited set of SST events (seven EP, five CP, and five DP El Niños), the ensemble of AMIP runs increases the sample size of atmospheric realizations. The approach has been commonly used to ensure that the atmospheric and terrestrial composites are not just an artifact of atmospheric internal variability and to confirm that observed composites are robust (e.g., Kumar and Hoerling 1995).

Since tropical precipitation acts as a forcing for the tropical–extratropical teleconnection via latent heat release, we first examine how differently tropical precipitation anomalies respond to the different types of El Niño SST (Figs. 3a–c) in the AMIP simulations. Figure 6 shows the composite of JJA seasonal mean tropical precipitation anomalies for different phases/patterns of El Niño from the multimodel ensemble of the 52 AMIP simulations. Associated with the EP El Niño, positive precipitation anomalies cross the central and eastern equatorial Pacific (Fig. 6a). Associated with the CP El Niño, precipitation anomalies are located in the western and central tropical Pacific (Fig. 6b) and have weaker amplitude. In the decaying phase of El Niño, significant positive precipitation anomalies are found near the coast of Central America (Fig. 6c). The changes in the tropical precipitation in the AMIP simulations are consistent with the changes in the tropical SST anomalies associated with the different phases/patterns of El Niño. Because the regions of tropical precipitation are also the regions where latent heat is released to the atmosphere, Fig. 6 indicates different locations of tropical heating associated with the different phases/patterns of El Niño for the atmosphere.

Figure 7 shows the composites of U.S. summer precipitation and surface air temperature anomalies from the multimodel ensemble of the 52 AMIP simulations. Model precipitation associated with each El Niño SST pattern (Figs. 3a–c) displays coherent continental-scale anomalies over the United States. The precipitation anomalies in response to both developing and decaying phases of El Niño (Figs. 7a,c) are closer to the observations (Figs. 3d,f) than that related to the CP El Niño (Figs. 7b and 3e). Similarly, the temperature anomalies during the developing and decaying phases of El Niño in the AMIP simulations (Figs. 7d,f) resemble the observations (Figs. 4a,c) more than that associated with the CP El Niño (Figs. 7e and 4b). Both precipitation and temperature display a center of maximum anomalies in the central United States in the developing phase of El Niño (Figs. 7a,d) and a north–south dipole in the decaying phase (Figs. 7c,f).

To quantify the similarity between the observations and AMIP simulations, Table 2 lists the pattern correlation between the observed and model simulated U.S. precipitation and surface temperature anomalies associated with different phases/patterns of El Niño. The pattern correlations are above the 99% significance level except for precipitation anomalies associated with the CP El Niños. Overall, the pattern correlations for U.S. precipitation and temperature anomalies during the developing phase of El Niño are higher than those during the decaying phase. The pattern correlations for the temperature anomalies are higher than for the precipitation anomalies. The results indicate that the AGCMs reproduce the observed precipitation and temperature anomalies associated with the developing phase of El Niño better than those associated with the decaying phase, and reproduce the observed temperature anomalies better than precipitation.

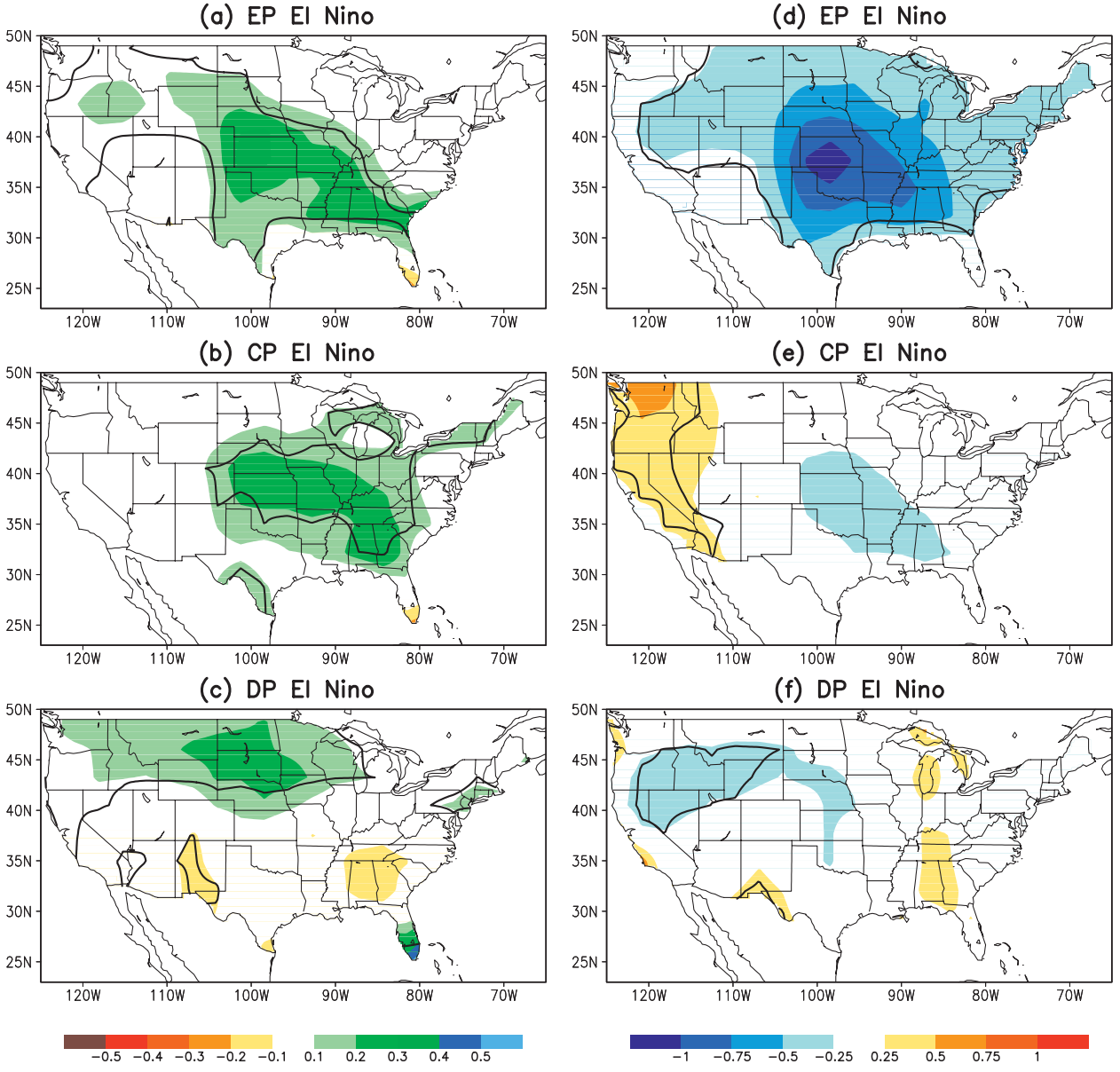


FIG. 7. As in Fig. 3, but for JJA seasonal mean U.S. (left) precipitation (mm day$^{-1}$) and (right) surface air temperature (°C) anomalies from the multimodel ensemble of 52 AMIP simulations.

To further assess the atmospheric response to different phases/patterns of El Niño, Fig. 8 shows the composite of 200-hPa geopotential height anomalies from the ensemble of the 52 AMIP simulations. Significant height anomalies are found in both the tropics and extratropics. In the developing phase of El Niño, the strongest tropical response is located between the date line and 120°W (Fig. 8a). The height response to the CP El Niño (Fig. 8b) is similar to that in the developing phase (Fig. 8a). It is also noted that the height response in the CP El Niño composite has larger positive amplitude even though the SST forcing itself has weaker amplitude (Figs. 3a,b). A similar feature is also true for the observed height composites (Figs. 5a,b). A stronger positive height anomaly associated with the CP El Niño is because a majority of years in the composite (i.e., four out of five) are after 1990 when an upward trend in height due to a general warming of tropical oceans has been observed (Kumar et al. 2004). A similar tendency for the La Niña height composites was discussed by Kumar et al. (2010).

During the decaying phase of El Niño, similar to the observations (Fig. 5c), there is a significant eastward shift of the maximum height anomalies along the equator

TABLE 2. Pattern correlations between observed and model-simulated U.S. precipitation, U.S. surface air temperature, and global 200-hPa height anomalies for the composites of the seven EP, five CP, and five DP El Niño years. All correlations are above the 99% significance level, estimated by the Monte Carlo test, except the correlation for precipitation anomalies in the CP El Niño composite.

| El Niño category | U.S. precipitation | U.S. temperature | 200-hPa height |
|---|---|---|---|
| EP (7 yr) | 0.52 | 0.85 | 0.70 |
| CP (5 yr) | 0.07 | 0.46 | 0.60 |
| DP (5 yr) | 0.34 | 0.74 | 0.65 |

(Fig. 8c) due to the eastward shift of the warm SST anomalies (Fig. 3c) and related tropical heating (Fig. 6c). The pattern correlations for the global 200-hPa height between the observations in Figs. 5a–c and the AMIP simulations in Figs. 8a–c are highly significant with correlation coefficients of 0.70, 0.60, and 0.65, respectively, also listed in Table 2. Therefore, the shift of SST anomalies (and associated tropical heating) and the atmospheric circulation response to this shift provide a physical explanation for the differences in the U.S. summer precipitation and temperature anomalies associated with the evolving and decaying phases of El Niño.

## 5. Summary

This study presented observational evidence of the differences in summer precipitation and temperature patterns in the United States associated with the developing and decaying phases of El Niño in the tropical Pacific. Using observational data, we found that the composite of U.S. summer precipitation anomalies for El Niño years is different from the composite of precipitation anomalies that covary with the El Niño SST based on singular value decomposition analysis (Ting and Wang 1997; Wang et al. 2010). Consistent with the precipitation composites, differences also exist in the surface air temperature. The analysis revealed that these differences in precipitation and temperature are related to differences in the SST patterns associated with El Niño. The U.S. summer precipitation and temperature anomalies in the decaying phase of El Niño, or following the peak phase of El Niño, are distinctive and stronger than those in the developing phase of El Niño.

Whether the differences in the U.S. summer precipitation and temperature anomalies before and after the peak phase of El Niño are the atmospheric responses to the changes in tropical SST—and associated heating—is assessed by analyzing the ensemble of 52 AMIP simulations with four AGCMs forced by the observed time-varying SST. The results of the multimodel ensemble

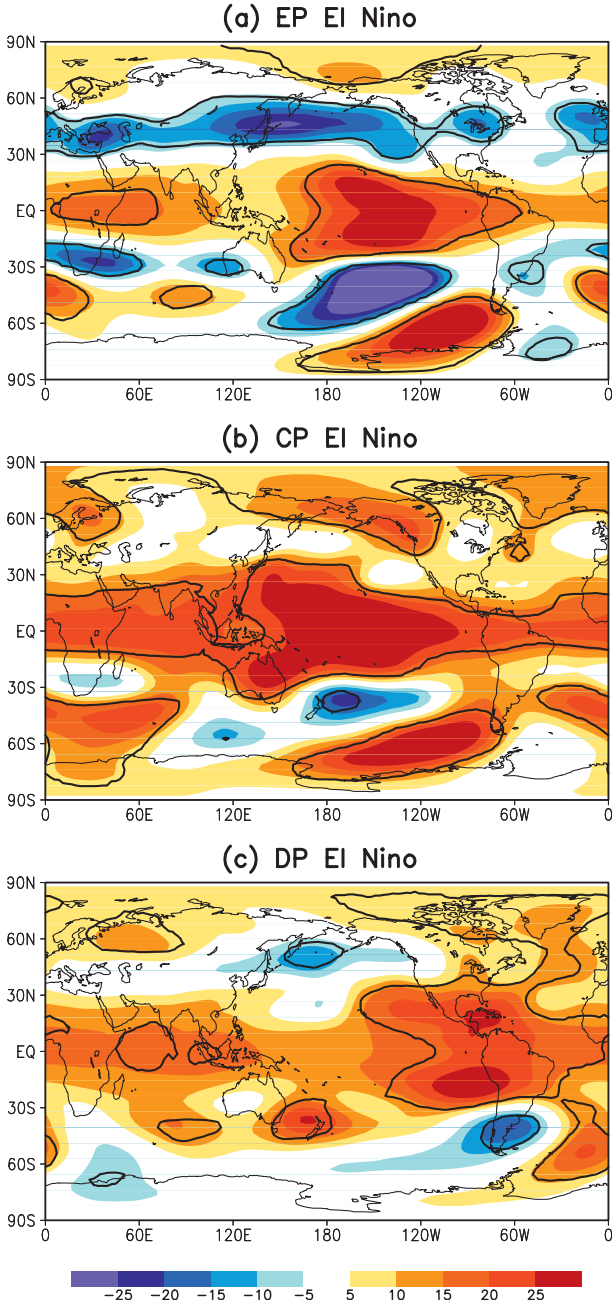


FIG. 8. As in Fig. 3, but for JJA seasonal mean global 200-hPa geopotential height anomaly (unit: gpm) from the multimodel ensemble of 52 AMIP simulations.

indicate that the U.S. precipitation and temperature responses to the tropical Pacific SST in the developing phase of El Niño are different from those in the decaying phase. Both are similar to the observations, though the amplitudes of the anomalies are smaller than the observations. The model response to the CP El Niño agrees less with the observations. The results suggest that the changes in the SST anomalies and associated tropical heating from

a growing El Niño to a decaying El Niño lead to different U.S. precipitation and temperature responses.

The ENSO evolution has a phase-locking behavior with respect to the annual cycle (Neelin et al. 2000). The peak phase of El Niño usually occurs in the winter season. The different characteristics of the U.S. summer precipitation before and after the peak phase of El Niño are consistent with previous studies that discussed the delayed atmospheric response to ENSO. Kumar and Hoerling (2003) found a stronger zonal mean 200-hPa circulation response over the tropics and subtropics in the summer following the winter ENSO than in the preceding summer. Indeed, a comparison of the 200-hPa height response based on AGCM simulations during the developing (Fig. 8a) and decaying (Fig. 8c) phase of El Niño clearly indicates a meridional broadening of the response, as was noted by Kumar and Hoerling (2003). Further, the magnitude of the 200-hPa height response during the decaying phase is not weaker than during the developing phase even though the area of warm SST anomalies is much smaller (Fig. 3c). The current study complements the finding of Kumar and Hoerling (2003) by considering the differences in U.S. summer precipitation and temperature anomalies in association with different phases of El Niño. A recent study by Ding et al. (2011) further suggests that, following the peak phase of winter El Niño, certain teleconnection patterns similar to those in Figs. 8a,c tend to occur in summer months.

The relationship between U.S. summer precipitation/temperature and El Niño and its difference between the developing and decaying phases of El Niño documented in this study suggest a source of potential predictability of summer precipitation and temperature associated with the evolution of El Niño. Given the large amplitudes of precipitation anomalies (Fig. 3f) and the distinctive pattern from the canonical pattern associated with El Niño (Fig. 1a), the tropical heating during the decaying phase of El Niño could be a forcing mechanism for the onset or cessation of U.S. summer droughts and floods. The results indicate an increase in the chances of heavy precipitation and flooding in the Missouri River basin and the Midwest during the summer following an El Niño winter. It is noted that the Great Flood of 1993 indeed occurred following the 1992/93 winter El Niño.

*Acknowledgments.* We thank Drs. Zeng-Zhen Hu and Scott Weaver, three anonymous reviewers, and the editor for their insightful and constructive comments and suggestions.

## REFERENCES

Ashok, K., S. K. Behera, S. A. Rao, H. Weng, and T. Yamagata, 2007: El Niño Modoki and its possible teleconnection. *J. Geophys. Res.,* **112,** C11007, doi:10.1029/2006JC003798.

Bacmeister, J., P. J. Pegion, S. D. Schubert, and M. J. Suarez, 2000: An atlas of seasonal means simulations by the NSIPP 1 atmospheric GCM. NASA Tech. Memo. 104606, Vol. 17, Goddard Space Flight Center, 194 pp.

Barnston, A. G., M. Chelliah, and S. B. Goldenberg, 1997: Documentation of a highly ENSO-related SST region in the equatorial Pacific. *Atmos.–Ocean,* **35,** 367–383.

Bretherton, C. S., C. Smith, and J. M. Wallace, 1992: An intercomparison of methods for finding coupled patterns in climate data. *J. Climate,* **5,** 541–560.

Bunkers, J. B., J. R. Miller, and A. T. DeGaetano, 1996: An examination of El Niño–La Niña-related precipitation and temperature anomalies across the Northern Plains. *J. Climate,* **9,** 147–160.

Delworth, T. L., and Coauthors, 2006: GFDL's CM2 global coupled climate models. Part I: Formulation and simulation characteristics. *J. Climate,* **19,** 643–674.

Ding, Q., B. Wang, J. M. Wallace, and G. Branstator, 2011: Tropical–extratropical teleconnections in boreal summer: Observed interannual variability. *J. Climate,* **24,** 1878–1896.

Higgins, R. W., W. Shi, E. Yarosh, and R. Joyce, cited 2000: Improved United States precipitation quality control system and analysis. [Available online at http://www.cpc.ncep.noaa.gov/research_papers/ncep_cpc_atlas/7/index. html.]

Kalnay, E., and Coauthors, 1996: The NCEP/NCAR 40-Year Reanalysis Project. *Bull. Amer. Meteor. Soc.,* **77,** 437–471.

Kumar, A., and M. P. Hoerling, 1995: Prospects and limitations of atmospheric GCM climate predictions. *Bull. Amer. Meteor. Soc.,* **76,** 335–345.

——, and ——, 2003: The nature and causes for the delayed atmospheric response to El Niño. *J. Climate,* **16,** 1391–1403.

——, F. Yang, L. Goddard, and S. Schubert, 2004: Differing trends in the tropical surface temperatures and precipitation over land and oceans. *J. Climate,* **17,** 653–664.

——, B. Jha, and M. L'Heureux, 2010: Are tropical SST trends changing the global teleconnection during La Niña? *Geophys. Res. Lett.,* **37,** L12702, doi:10.1029/2010GL043394.

Neelin, J. D., F.-F. Jin, and H.-H. Syu, 2000: Variations in ENSO phase locking. *J. Climate,* **13,** 2570–2590.

Roeckner, E., and Coauthors, 1996: The atmospheric general circulation model ECHAM4: Model description and simulation of present day climate. Rep. 218, Max-Planck-Institute fur Meteorologie, 90 pp.

Ropelewski, C. F., and M. S. Halpert, 1986: North American precipitation and temperature patterns associated with the El Niño/Southern Oscillation (ENSO). *Mon. Wea. Rev.,* **114,** 2352–2362.

——, and ——, 1987: Global and regional scale precipitation patterns associated with El Niño/Southern Oscillation. *Mon. Wea. Rev.,* **115,** 1606–1626.

Saha, S., and Coauthors, 2010: The NCEP Climate Forecast System reanalysis. *Bull. Amer. Meteor. Soc.,* **91,** 1015–1057.

Smith, T. M., R. W. Reynolds, T. C. Peterson, and J. Lawrimore, 2008: Improvements to NOAA's historical merged land–ocean surface temperature analysis (1880–2006). *J. Climate,* **21,** 2283–2293.

Ting, M., and H. Wang, 1997: Summertime U.S. precipitation variability and its relation to Pacific sea surface temperature. *J. Climate,* **10,** 1853–1873.

Trenberth, K. E., 1997: The definition of El Niño. *Bull. Amer. Meteor. Soc.,* **78,** 2771–2777.

——, and C. J. Guillemot, 1996: Physical processes involved in the 1988 drought and 1993 floods in North America. *J. Climate,* **9,** 1288–1298.

Wang, H., R. Fu, A. Kumar, and W. Li, 2010: Intensification of summer rainfall variability in the southeastern United States during recent decades. *J. Hydrometeor.,* **11,** 1007–1018.

Weaver, S. J., S. Schubert, and H. Wang, 2009: Warm season variations in the low-level circulation and precipitation over the central United States in observations, AMIP simulations, and idealized SST experiments. *J. Climate,* **22,** 5401–5420.

Wilks, D. S., 1995: *Statistical Methods in the Atmospheric Sciences*. Academic Press, 467 pp.

Yeh, S.-W., J.-S. Kug, B. Dewitte, M.-H. Kwon, B. P. Kirtman, and F.-F. Jin, 2009: El Niño in a changing climate. *Nature,* **461,** 511–514.

Zhao, W., and M. A. K. Khalil, 1993: The relationship between precipitation and temperature over the contiguous United States. *J. Climate,* **6,** 1232–1236.